Networks and Heterogeneous Media

https://www.aimspress.com/journal/nhm

NHM, 21(1): 324–348.
DOI: 10.3934/nhm.2026015
Received: 05 December 2025
Revised: 03 March 2026
Accepted: 04 March 2026
Published: 18 March 2026

Research article

A linearly implicit local energy-dissipative method for the generalized nonlinear wave equation

Yulian Yi[1], **Yuchen Yin**[2] **and Mingfa Fei**[1,*]

[1] School of Mathematics, Changsha University, Changsha 410022, China

[2] Teachers College, Columbia University, New York 10027, USA

* **Correspondence:** Email: mingfa_fei@163.com.

Abstract: In this paper, we propose a linearly implicit scheme that preserves the local energy dissipation property for the generalized nonlinear wave equation. By employing the energy quadratization approach, we reformulated the original equation into an equivalent form. A semi-discrete structure-preserving system was constructed via finite difference discretization in space. Subsequently, we derived a fully discretized scheme using the Crank-Nicolson method combined with the extrapolation technique, ensuring the preservation of local energy dissipation law. Under appropriate boundary conditions, such as homogeneous Dirichlet or periodic boundary conditions, the proposed method also maintained the global energy dissipation law. Furthermore, the unique solvability, fast implementation, and convergence theorem of the discrete scheme were analyzed rigorously. Numerical experiments are presented to validate our theoretical results, demonstrating that the proposed scheme outperforms traditional methods in terms of stability and efficiency.

Keywords: nonlinear wave equation; linearly implicit scheme; structure-preserving method; local energy dissipation law; convergence analysis

1. Introduction

The generalized nonlinear wave equation refers to a form of wave equation that incorporates nonlinearity, typically in the form of nonlinear terms that modify the standard wave equation. These nonlinearity terms can arise from various physical effects such as nonlinear material properties, large amplitude wave interactions, or other complex phenomena in fields such as fluid dynamics, acoustics, or elastodynamics [1–5]. A general form of a nonlinear wave equation can be written as in [6].

$$u_{tt} - \Delta u + \beta u_t + f(u) = 0, \quad \boldsymbol{x} \in \Omega, \quad 0 < t \leq T, \tag{1.1}$$

with the initial value conditions

$$u(\boldsymbol{x},0)=\eta(\boldsymbol{x}),\quad u_t(\boldsymbol{x},0)=\phi(\boldsymbol{x}),\quad \boldsymbol{x}\in\Omega, \tag{1.2}$$

where $\Omega=(x_L,x_R)\times(y_L,y_R)$, η and ϕ are given smooth functions and β represents the nonnegative damping force. $f(u)$ is a nonlinear source term that depends on the wave field u, which satisfies $f(u)=F'(u)$, and $|\partial_u f(u)|$ is bounded.

By setting $u_t=v$, the original second-order system can be expressed equivalently as

$$u_t=v, \tag{1.3}$$

$$v_t=\Delta u-\beta u_t-f(u). \tag{1.4}$$

Proposition 1.1. The nonlinear wave equation (1.1) conserves the following local energy dissipation law

$$\Big(\frac{1}{2}v^2+\frac{1}{2}(u_x^2+u_y^2)+F(u)\Big)_t-\big((u_xv)_x+(u_yv)_y\big)=-\beta v^2\le 0. \tag{1.5}$$

Proof. By multiplying Eq (1.4) by v, we obtain

$$vv_t-\Delta uv+f(u)v=-\beta v^2. \tag{1.6}$$

Applying the continuous Leibniz rule and using Eq (1.3), we get

$$vv_t=\frac{1}{2}(v^2)_t,\quad f(u)v=f(u)u_t=(F(u))_t. \tag{1.7}$$

For the term Δuv, we can rewrite it as

$$\Delta uv=(u_xv)_x+(u_yv)_y-\frac{1}{2}(u_x^2+u_y^2)_t. \tag{1.8}$$

Combining the results from Eqs (1.6)–(1.8), we derive the local energy dissipation law given by Eq (1.5).

Denote $\|u\|:=\sqrt{(u,u)}=\sqrt{\int_\Omega u^2d\boldsymbol{x}}$. With appropriate boundary conditions such as homogeneous Dirichlet or periodic boundary conditions, it holds that $\int_\Omega((u_xv)_x+(u_yv)_y)d\boldsymbol{x}=0$. Therefore, by applying the local energy dissipation law (1.5) across the spatial domain yields the corresponding global energy dissipation law, namely

$$\frac{d\mathcal{H}}{dt}=-\beta\|v\|^2\le 0,\quad t\in[0,T], \tag{1.9}$$

where the Hamiltonian energy functional $\mathcal{H}(t)$ is defined as

$$\mathcal{H}(t)=\int_\Omega\Big(\frac{1}{2}v^2+\frac{1}{2}(u_x^2+u_y^2)+F(u)\Big)d\boldsymbol{x}. \tag{1.10}$$

In particular, the energy of model (1.1) is conserved when $\beta=0$, it preserves the local energy conservation law $(\frac{1}{2}v^2+\frac{1}{2}(u_x^2+u_y^2)+F(u))_t-((u_xv)_x+(u_yv)_y)=0$, and maintains the global energy conservation law $\mathcal{H}(t)\equiv\mathcal{H}(0)$ $(t>0)$ under appropriate boundary conditions such as homogeneous Dirichlet or periodic boundary conditions.

The generalized nonlinear wave equation typically involves highly nonlinear terms that substantially increase the complexity to the behavior of system. These nonlinearities can lead to a wide range of dynamic phenomena, such as shock waves, pattern formation, and multiscale interactions, making the derivation of analytical solutions particularly difficult. To address these challenges, numerical methods have been developed for solving the generalized nonlinear wave equation such as the finite element method for spatial discretization coupled with implicit time-stepping schemes [7, 8], the pseudo-spectral method for high-accuracy solutions in complex domains [9, 10]. And, Zhao and Gu [11] proposed a low-rank solution method for the strongly damped wave equation. Luo et al. [12] constructed a Bernoulli-barycentric rational matrix collocation method for two-dimensional evolutionary PDEs. These approaches provide efficient tools for capturing the intricate dynamics of the generalized nonlinear wave equation under boundary and initial conditions. Energy dissipation is a fundamental characteristic for many physical systems, particularly in scenarios involving damping or friction. This is crucial for elucidating how energy is progressively lost and for evaluating long-term stability [13, 14]. Precise modeling of energy dissipation is vital to ensure numerical methods accurately replicate physical behavior, especially in studies of wave attenuation and thermal diffusion [15, 16]. However, many numerical methods fail to adequately preserve the discrete energy dissipation law, which can result in unrealistic long-term behavior and inaccurate representation of damping effects.

Structure-preserving algorithms, particularly symplectic integrators, are designed to preserve key properties of dynamical systems during simulations [17–21]. These methods are especially useful for Hamiltonian systems, which arise ubiquitously in molecular dynamics, celestial mechanics, and fluid dynamics, where maintaining energy, momentum, or other invariants over long time periods is essential [22–24]. There have been substantial advancements in the development of structure-preserving methods, such as the discrete gradient method [25], averaged vector field method (AVF) [26], and Crank-Nicolson scheme [27, 28]. For nonlinear wave equations, Jiang et al. proposed a high-order structure-preserving scheme based on the AVF method [14]. Macías-Díaz and his colleagues introduced an energy function for the nonlocal wave equation with the Riesz fractional derivative, and analyzed a series of energy-dissipation (or conservation) schemes [29–31]. Additionally, the researchers in [32–34] constructed some dissipation-preserving finite difference schemes for wave equations. Other related structure-preserving methods are detailed in Refs. [35, 36].

The energy quadratization (EQ) method [37–40] has been developed to construct linearly implicit energy-stable schemes for gradient flows. By integrating the extrapolation technique, symplectic Runge-Kutta (RK) method [41, 42], and EQ approach, efficient and high-accuracy schemes for conservative/dissipative systems have been achieved [43, 44]. However, these schemes are limited to preserving global energy, which is dependent on boundary conditions such as periodic boundaries. In the absence of such conditions, their effectiveness is considerably diminished. To overcome this limitation, Wang et al. [45] introduced the idea of local structure-preserving methods. This approach extends the conserved structures from global methods to local regions, ensuring that these structures are maintained in any local area or point within the time-space domain, which eliminates the need for specific boundary conditions. Local structure-preserving methods have gained significant attention in the study of Hamiltonian PDEs [46–48].

However, most nonlocal structure-preserving algorithms are fully implicit schemes, which require nonlinear iterations in long-term numerical simulations and thus incur substantial computational

costs. Linear implicit schemes exhibit exceptional computational efficiency in numerical simulations. Nevertheless, to the best of our knowledge, linearly implicit schemes that preserve local energy dissipation laws for the generalized nonlinear wave equation have not been explored. Moreover, establishing a convergence theorem for such a method without imposing a time-space grid ratio constraint remains a significant challenge. In this paper, we aim to develop a linearly implicit scheme based on the EQ technique that preserves local energy dissipation for the system (1.1). The major contributions of this study are as follows:

- We construct a new linear, second-order scheme for the generalized nonlinear wave equation based on the energy quadratization strategy, Crank-Nicolson method, and extrapolation technique.
- The discrete scheme preserves the local energy dissipation law as the continuous mode, and also maintains the global energy dissipation law under appropriate boundary conditions.
- A thorough analysis of the proposed method is established, including unique solvability, fast implementation, and the unconditional convergence theorem.

This paper is structured as follows: In Section 2, we introduce a new auxiliary variable to derive an equivalent system that includes local and global modified energy dissipation laws as a continuous model. In Section 3, a linearly implicit scheme is proposed, which utilizes the extrapolation technique and finite difference methods to discretize time and space variables. Additionally, a fast solver for the scheme is developed. In Section 4, we offer a thorough analysis of the proposed scheme, including unique solvability and convergence results. In Section 5, we present numerical experiments that validate our theoretical analysis. Finally, in Section 6, we summarize the major findings and provide key insights.

2. Model reformulation

In this section, we use the EQ approach to obtain an equivalent system for the nonlinear wave equation. Following the ideas proposed in [37–39], we introduce an auxiliary variable

$$r(u,t) = \sqrt{F(u) + C_0}. \tag{2.1}$$

Here, $C_0 > 0$ is a constant that ensures the well-defined nature of $r(u,t)$, i.e., $F(u) + C_0 > 0$. Then, systems (1.3) and (1.4) can be reformulated as a new equivalent system, namely

$$u_t = v, \tag{2.2}$$

$$v_t = \Delta u - \beta u_t - \frac{f(u)}{\sqrt{F(u) + C_0}} r, \tag{2.3}$$

$$r_t = \frac{1}{2} \frac{f(u)}{\sqrt{F(u) + C_0}} u_t, \tag{2.4}$$

with

$$r_0 := \sqrt{F(u_0) + C_0}. \tag{2.5}$$

Next, we study the energy dissipation properties of the rephrased EQ systems (2.2)–(2.4). To this end, the following modified energy function $\mathcal{E}(t)$ is introduced as

$$\mathcal{E}(t) = \int_\Omega (\frac{1}{2} v^2 + \frac{1}{2}(u_x^2 + u_y^2) + r^2) d\boldsymbol{x}. \tag{2.6}$$

Theorem 2.1. *The EQ systems* (2.2)–(2.4) *possesses the modified local energy dissipation law*

$$(\frac{1}{2}v^2 + \frac{1}{2}(u_x^2 + u_y^2) + r^2)_t - ((u_x v)_x + (u_y v)_y) = -\beta v^2 \leq 0. \tag{2.7}$$

Under appropriate boundary conditions, such as homogeneous Dirichlet or periodic boundary conditions, EQ systems (2.2)–(2.4) *also preserve the modified global energy dissipation law*

$$\frac{d\mathcal{E}(t)}{dt} = -\beta\|v\|^2 \leq 0. \tag{2.8}$$

Proof. By multiplying Eq (2.3) by v, we obtain

$$vv_t - \Delta uv + \frac{f(u)}{\sqrt{F(u) + C_0}} rv = -\beta v^2. \tag{2.9}$$

Multiplying Eq (2.4) by $2r$ can yield

$$\frac{d}{dt}r^2 = \frac{f(u)}{\sqrt{F(u) + C_0}} ru_t. \tag{2.10}$$

In view of Eqs (1.7), (1.8), (2.9), and (2.10), we can derive the modified local energy dissipation law (2.7).

With appropriate boundary conditions, including homogeneous Dirichlet or periodic boundary conditions, integrating Eq (2.7) across the spatial domain indicates the corresponding global energy dissipation law

$$\frac{d\mathcal{E}(t)}{dt} = \frac{d}{dt}\int_\Omega (\frac{1}{2}v^2 + \frac{1}{2}(u_x^2 + u_y^2) + r^2)d\boldsymbol{x} = -\beta\|v\|^2 \leq 0. \tag{2.11}$$

We complete the proof.

Remark 2.1. *We mention that when $\beta = 0$, the equivalent systems* (2.2)–(2.4) *preserves the modified local energy conservation law $(\frac{1}{2}v^2 + \frac{1}{2}(u_x^2 + u_y^2) + r^2)_t - ((u_x v)_x + (u_y v)_y) \equiv 0$. Besides, the modified global energy conservation law $\frac{d\mathcal{E}(t)}{dt} \equiv 0$ also holds under homogeneous Dirichlet or periodic boundary conditions.*

3. Construction of the linearly implicit and local structure-preserving scheme

In this section, we construct a linearly implicit local energy-dissipative scheme. First, some fundamental concepts and definitions are introduced, which will be used in the subsequent proofs. Let $\Omega_h = \{(x_i, y_j) \mid x_i = x_L + ih_x,\ y_j = y_L + jh_y;\ 1 \leq i \leq N_x - 1,\ 1 \leq j \leq N_y - 1\}$ represent a partition of Ω with the mesh sizes $h_x = (x_R - x_L)/N_x$ and $h_y = (y_R - y_L)/N_y$, where N_x and N_y are given even numbers.

For a positive integer N, let $\Omega_\tau = \{t_n \mid t_n = n\tau;\ 0 \le n \le N\}$ be a uniform partition of $[0, T]$ with a time step $\tau = T/N$. Then, $\Omega_{\tau h} = \Omega_h \times \Omega_\tau$, and let $z^n_{i,j}$ be a mesh function defined over $\Omega_{\tau h}$. We denote

$$\delta_t z^n_{ij} = \frac{z^{n+1}_{ij} - z^n_{ij}}{\tau}, \quad \rho_t z^n_{ij} = \frac{z^{n+1}_{ij} + z^n_{ij}}{2}, \quad \hat{z}^n_{ij} = \frac{3z^n_{ij} - z^{n-1}_{ij}}{2},$$
$$\delta^\pm_x z^n_{ij} = \pm\frac{z^n_{i\pm1,j} - z^n_{i,j}}{h_x}, \quad \delta^2_x z^n_{ij} = \frac{z^n_{i+1,j} - 2z^n_{i,j} + z^n_{i-1,j}}{h^2_x},$$
$$\delta^\pm_y z^n_{ij} = \pm\frac{z^n_{i,j\pm1} - z^n_{i,j}}{h_y}, \quad \delta^2_y z^n_{ij} = \frac{z^n_{i,j+1} - 2z^n_{i,j} + z^n_{i,j-1}}{h^2_y}.$$

The commutative law states that:

$$\delta_t\delta^\pm_x z^n_{ij} = \delta^\pm_x\delta_t z^n_{ij}, \quad \rho_t\delta^\pm_y z^n_{ij} = \delta^\pm_y\rho_t z^n_{ij}, \quad \delta^+_x\delta^-_x z^n_{ij} = \delta^-_x\delta^+_x z^n_{ij} = \delta^2_x z^n_{ij}, \quad \delta^+_y\delta^-_y z^n_{ij} = \delta^-_y\delta^+_y z^n_{ij} = \delta^2_y z^n_{ij}.$$

The discrete Leibniz rule includes:

$$(a) \quad \delta_t(z^n_{ij}v^n_{ij}) = \rho_t z^n_{ij}\delta_t v^n_{ij} + \delta_t z^n_{ij}\rho_t v^n_{ij},$$
$$(b) \quad \delta_t(z^n_{ij}v^n_{ij}) = \delta_t z^n_{ij}\cdot v^n_{ij} + z^{n+1}_{ij}\delta_t v^n_{ij},$$
$$(c) \quad \delta_t(z^n_{ij}v^n_{ij}) = \delta_t z^n_{ij}\cdot v^{n+1}_{ij} + z^n_{ij}\delta_t v^n_{ij}.$$

The above rules are also applicable for the operators δ^+_x and δ^+_y.

To simplify notation, let $z^n_{ij} = z(x_i, y_j, t_n)$, and denote $\boldsymbol{z}_{ij}$ and $\boldsymbol{z}^n_{ij}$ as the numerical approximations of $z(x_i, y_j, t)$ and $z(x_i, y_j, t_n)$, respectively. Let

$$\mathcal{Z}_h := \{z \mid z = (\boldsymbol{z}_{1,1}, \boldsymbol{z}_{2,1}, \cdots, \boldsymbol{z}_{N_x-1,1}, \cdots, \boldsymbol{z}_{1,N_y-1}, \boldsymbol{z}_{2,N_y-1}, \cdots, \boldsymbol{z}_{N_x-1,N_y-1})^T\}$$

be the space of mesh functions on Ω_h that satisfy periodic boundary conditions. For any $\boldsymbol{u}, \boldsymbol{v} \in \mathcal{Z}_h$, the discrete inner products are defined as

$$\langle \boldsymbol{u}, \boldsymbol{v}\rangle = h_x h_y \sum_{i=1}^{N_x-1}\sum_{j=1}^{N_y-1} \boldsymbol{u}_{i,j}\boldsymbol{v}_{i,j},$$

and

$$\langle \delta_\theta\boldsymbol{u}, \delta_\theta\boldsymbol{v}\rangle = h_x h_y \sum_{i=1}^{N_x-1}\sum_{j=1}^{N_y-1} \delta_\theta\boldsymbol{u}_{i,j}\delta_\theta\boldsymbol{v}_{i,j},$$

where $\theta = x, y$ indicates the spatial directions. The discrete L^2-norm of $\boldsymbol{u} \in \mathcal{Z}_h$ and the norms of its difference quotients are given as

$$\|\boldsymbol{u}\| = \sqrt{\langle \boldsymbol{u}, \boldsymbol{u}\rangle}, \quad \|\delta^+_x\boldsymbol{u}\| = \sqrt{\langle \delta^+_x\boldsymbol{u}, \delta^+_x\boldsymbol{u}\rangle}, \quad \|\delta^+_y\boldsymbol{u}\| = \sqrt{\langle \delta^+_y\boldsymbol{u}, \delta^+_y\boldsymbol{u}\rangle}.$$

We further define the discrete H^1_h-norm and L^∞-norm as:

$$\|\boldsymbol{u}\|_{H^1_h} = \sqrt{\|\boldsymbol{u}\|^2 + \|\delta^+_x\boldsymbol{u}\|^2 + \|\delta^+_y\boldsymbol{u}\|^2}, \quad \|\boldsymbol{u}\|_\infty = \max_{\substack{0<i<N_x\\ 0<j<N_y}} \left|\boldsymbol{u}_{i,j}\right|.$$

For simplicity, the componentwise product $\boldsymbol{u}\cdot\boldsymbol{v}$ is given by

$$\boldsymbol{u}\cdot\boldsymbol{v} = \left(\boldsymbol{u}_{1,1}\boldsymbol{v}_{1,1}, \cdots, \boldsymbol{u}_{N_x-1,1}\boldsymbol{v}_{N_x-1,1}, \cdots, \boldsymbol{u}_{1,N_y-1}\boldsymbol{v}_{1,N_y-1}, \cdots, \boldsymbol{u}_{N_x-1,N_y-1}\boldsymbol{v}_{N_x-1,N_y-1}\right)^T.$$

3.1. Local energy-dissipative space semi-discretization

Structure-preserving schemes have been developed for solving the nonlinear wave equation. However, the local energy-dissipative scheme associated with spatial discretization has received less attention. In this section, we employ the conventional finite difference method for spatial discretization and demonstrate that the resulting semi-discrete system precisely maintains the semi-discrete local energy dissipation law.

By applying the finite difference method to the spatial discretization of systems (2.2)–(2.4), we obtain the following semi-discrete system

$$\frac{d\boldsymbol{u}_{ij}}{dt} = \boldsymbol{v}_{ij}, \tag{3.1}$$

$$\frac{d\boldsymbol{v}_{ij}}{dt} = \delta_x^2\boldsymbol{u}_{ij} + \delta_y^2\boldsymbol{u}_{ij} - \beta\boldsymbol{v}_{ij} - \frac{f(\boldsymbol{u}_{ij})}{\sqrt{F(\boldsymbol{u}_{ij}) + C_0}}\boldsymbol{r}_{ij}, \tag{3.2}$$

$$\frac{d\boldsymbol{r}_{ij}}{dt} = \frac{1}{2}\frac{f(\boldsymbol{u}_{ij})}{\sqrt{F(\boldsymbol{u}_{ij}) + C_0}}\frac{d\boldsymbol{u}_{ij}}{dt}. \tag{3.3}$$

Theorem 3.1. *The space semi-discrete systems* (3.1)–(3.3) *conserves the modified local energy dissipation law*

$$\frac{d}{dt}\Big(\frac{1}{2}\boldsymbol{v}_{ij}^2 + \frac{1}{2}((\delta_x^+\boldsymbol{u}_{ij})^2 + (\delta_y^+\boldsymbol{u}_{ij})^2) + \boldsymbol{r}_{ij}^2\Big) - \Big(\delta_x^+(\delta_x^-\boldsymbol{u}_{ij}\cdot\boldsymbol{v}_{ij}) + \delta_y^+(\delta_y^-\boldsymbol{u}_{ij}\cdot\boldsymbol{v}_{ij})\Big) \le 0. \tag{3.4}$$

Furthermore, with appropriate boundary conditions such as homogeneous Dirichlet or periodic boundary conditions, the semi-discrete systems (3.1)–(3.3) *also possesses the following modified global energy dissipation law*

$$\frac{dE(t)}{dt} \le 0, \tag{3.5}$$

where $E(t)$ *is given*

$$E(t) = \frac{1}{2}\langle\boldsymbol{v},\boldsymbol{v}\rangle + \frac{1}{2}(\langle\delta_x^+\boldsymbol{u},\delta_x^+\boldsymbol{u}\rangle + \langle\delta_y^+\boldsymbol{u},\delta_y^+\boldsymbol{u}\rangle) + \langle\boldsymbol{r},\boldsymbol{r}\rangle. \tag{3.6}$$

Proof. By multiplying Eq (3.2) by $\boldsymbol{v}_{ij}$, we obtain

$$\frac{d\boldsymbol{v}_{ij}}{dt}\boldsymbol{v}_{ij} = (\delta_x^2\boldsymbol{u}_{ij} + \delta_y^2\boldsymbol{u}_{ij})\boldsymbol{v}_{ij} - \beta\boldsymbol{v}_{ij}^2 - \frac{f(\boldsymbol{u}_{ij})}{\sqrt{F(\boldsymbol{u}_{ij}) + C_0}}\boldsymbol{r}_{ij}\boldsymbol{v}_{ij}. \tag{3.7}$$

Next, multiplying Eq (3.3) by $2\boldsymbol{r}_{ij}$ yields

$$\frac{d}{dt}\boldsymbol{r}_{ij}^2 = \frac{f(\boldsymbol{u}_{ij})\boldsymbol{r}_{ij}}{\sqrt{F(\boldsymbol{u}_{ij}) + C_0}}\frac{d\boldsymbol{u}_{ij}}{dt} = \frac{f(\boldsymbol{u}_{ij})}{\sqrt{F(\boldsymbol{u}_{ij}) + C_0}}\boldsymbol{r}_{ij}\boldsymbol{v}_{ij}. \tag{3.8}$$

Using the discrete Leibniz rule, we can derive the following results

$$\begin{aligned}\delta_x^2\boldsymbol{u}_{ij}\cdot\boldsymbol{v}_{ij} &= \delta_x^+(\delta_x^-\boldsymbol{u}_{ij}\cdot\boldsymbol{v}_{ij}) - (\delta_x^+\boldsymbol{u}_{ij}\cdot\boldsymbol{v}_{i+1,j} - \delta_x^+\boldsymbol{u}_{ij}\cdot\boldsymbol{v}_{i,j})\\ &= \delta_x^+(\delta_x^-\boldsymbol{u}_{ij}\cdot\boldsymbol{v}_{ij}) - \delta_x^+\boldsymbol{u}_{ij}\delta_x^+\boldsymbol{v}_{i,j}\end{aligned}$$

$$= \delta_x^+(\delta_x^- \boldsymbol{u}_{ij} \cdot \boldsymbol{v}_{ij}) - \delta_x^+ \boldsymbol{u}_{ij} \delta_x^+ \frac{d\boldsymbol{u}_{ij}}{dt}$$
$$= \delta_x^+(\delta_x^- \boldsymbol{u}_{ij} \cdot \boldsymbol{v}_{ij}) - \frac{1}{2}\frac{d}{dt}(\delta_x^+ \boldsymbol{u}_{ij})^2. \tag{3.9}$$

Similarly, we have

$$\delta_y^2 \boldsymbol{u}_{ij} \cdot \boldsymbol{v}_{ij} = \delta_y^+(\delta_y^- \boldsymbol{u}_{ij} \cdot \boldsymbol{v}_{ij}) - \frac{1}{2}\frac{d}{dt}(\delta_y^+ \boldsymbol{u}_{ij})^2. \tag{3.10}$$

From Eqs (3.7)–(3.10), we can obtain the local energy dissipation law

$$\frac{d}{dt}\left(\frac{1}{2}\boldsymbol{v}_{ij}^2 + \frac{1}{2}((\delta_x^+ \boldsymbol{u}_{ij})^2 + (\delta_y^+ \boldsymbol{u}_{ij})^2) + \boldsymbol{r}_{ij}^2\right) - \left(\delta_x^+(\delta_x^- \boldsymbol{u}_{ij} \cdot \boldsymbol{v}_{ij}) + \delta_y^+(\delta_y^- \boldsymbol{u}_{ij} \cdot \boldsymbol{v}_{ij})\right) = -\beta \boldsymbol{v}_{ij}^2 \le 0. \tag{3.11}$$

Under homogeneous Dirichlet boundary condition, based on the discrete summation-by-parts identities it can be deduced that

$$\sum_{i=1}^{N_x-1}\sum_{j=1}^{N_y-1}\left(\delta_x^+(\delta_x^- \boldsymbol{u}_{ij} \cdot \boldsymbol{v}_{ij}) + \delta_y^+(\delta_y^- \boldsymbol{u}_{ij} \cdot \boldsymbol{v}_{ij})\right) = 0.$$

Therefore, summing Eq (3.11) over spatial grid points leads to the global energy dissipation law

$$\frac{d}{dt}\left(\frac{1}{2}\langle \boldsymbol{v}, \boldsymbol{v}\rangle + \frac{1}{2}(\langle \delta_x^+ \boldsymbol{u}, \delta_x^+ \boldsymbol{u}\rangle + \langle \delta_y^+ \boldsymbol{u}, \delta_y^+ \boldsymbol{u}\rangle) + \langle \boldsymbol{r}, \boldsymbol{r}\rangle\right) = -\beta\|\boldsymbol{v}\|^2 \le 0. \tag{3.12}$$

For the periodic boundary condition case, a similar conclusion can be established.
This ends the proof of this theorem.

3.2. The fully discrete linearly implicit and local energy-dissipative scheme

Now we derive a fully discrete scheme by applying the linearly implicit structure-preserving time discretization to the semi-discrete systems (3.1)–(3.3), which is denoted as the **LILED** scheme, namely

$$\delta_t \boldsymbol{u}_{ij}^n = \rho_t \boldsymbol{v}_{ij}^n, \tag{3.13}$$
$$\delta_t \boldsymbol{v}_{ij}^n = \delta_x^2 \rho_t \boldsymbol{u}_{ij}^n + \delta_y^2 \rho_t \boldsymbol{u}_{ij}^n - \beta \rho_t \boldsymbol{v}_{ij}^n - \frac{f(\hat{\boldsymbol{u}}_{ij}^n)}{\sqrt{F(\hat{\boldsymbol{u}}_{ij}^n) + C_0}} \rho_t \boldsymbol{r}_{ij}^n, \tag{3.14}$$
$$\delta_t \boldsymbol{r}_{ij}^n = \frac{1}{2}\frac{f(\hat{\boldsymbol{u}}_{ij}^n)}{\sqrt{F(\hat{\boldsymbol{u}}_{ij}^n) + C_0}} \rho_t \boldsymbol{v}_{ij}^n. \tag{3.15}$$

Remark 3.1. The **LILED** scheme described in Eqs (3.13)–(3.15) is a three-level method. For the initial step, we calculate $\boldsymbol{u}_{ij}^1$, $\boldsymbol{v}_{ij}^1$ and $\boldsymbol{r}_{ij}^1$ using $\boldsymbol{u}_{ij}^0$ instead of $\hat{\boldsymbol{u}}_{ij}^0$ as shown in Eqs (3.14) and (3.15). Although this scheme is presented for the two-dimensional nonlinear wave equation, it can be extended to one-dimensional and three-dimensional cases.

Theorem 3.2. *The fully-discrete* **LILED** *scheme* (3.13)–(3.15) *conserves the modified local energy dissipation law*

$$\delta_t\Big(\frac{1}{2}(\boldsymbol{v}_{ij}^n)^2+\frac{1}{2}((\delta_x^+\boldsymbol{u}_{ij}^n)^2+(\delta_y^+\boldsymbol{u}_{ij}^n)^2)+(\boldsymbol{r}_{ij}^n)^2\Big)-\Big(\delta_x^+\left(\rho_t\delta_x^-\boldsymbol{u}_{ij}^n\cdot\rho_t\boldsymbol{v}_{ij}^n\right)+\delta_y^+\left(\rho_t\delta_y^-\boldsymbol{u}_{ij}^n\cdot\rho_t\boldsymbol{v}_{ij}^n\right)\Big)=-\beta(\rho_t\boldsymbol{v}_{ij}^n)^2\le 0. \tag{3.16}$$

With appropriate boundary conditions such as homogeneous Dirichlet or periodic boundary conditions, the discrete **LILED** *scheme also preserves the modified global energy dissipation law, namely*

$$E^N\le E^{N-1}\le\cdots\le E^0, \tag{3.17}$$

where

$$E^n=\frac{1}{2}\langle\boldsymbol{v}^n,\boldsymbol{v}^n\rangle+\frac{1}{2}(\langle\delta_x^+\boldsymbol{u}^n,\delta_x^+\boldsymbol{u}^n\rangle+\langle\delta_y^+\boldsymbol{u}^n,\delta_y^+\boldsymbol{u}^n\rangle)+\langle\boldsymbol{r}^n,\boldsymbol{r}^n\rangle,\quad n=0,1,\cdots,N. \tag{3.18}$$

Proof. By multiplying Eq (3.14) by $\rho_t\boldsymbol{v}_{ij}^n$, we obtain

$$\rho_t\boldsymbol{v}_{ij}^n\delta_t\boldsymbol{v}_{ij}^n=\rho_t\boldsymbol{v}_{ij}^n(\delta_x^2\rho_t\boldsymbol{u}_{ij}^n+\delta_y^2\rho_t\boldsymbol{u}_{ij}^n)-\beta(\rho_t\boldsymbol{v}_{ij}^n)^2-\frac{f(\hat{\boldsymbol{u}}_{ij}^n)}{\sqrt{F(\hat{\boldsymbol{u}}_{ij}^n)+C_0}}\rho_t\boldsymbol{r}_{ij}^n\rho_t\boldsymbol{v}_{ij}^n. \tag{3.19}$$

Then, multiplying Eq (3.15) by $\rho_t\boldsymbol{r}^n$ yields

$$\rho_t\boldsymbol{r}_{ij}^n\delta_t\boldsymbol{r}_{ij}^n=\frac{1}{2}\delta_t(\boldsymbol{r}_{ij}^n)^2=\frac{1}{2}\frac{f(\hat{\boldsymbol{u}}_{ij}^n)}{\sqrt{F(\hat{\boldsymbol{u}}_{ij}^n)+C_0}}\rho_t\boldsymbol{v}_{ij}^n\rho_t\boldsymbol{r}_{ij}^n. \tag{3.20}$$

Using the commutative law and the discrete Leibniz rule, we can derive

$$\delta_t\boldsymbol{v}_{ij}^n\cdot\rho_t\boldsymbol{v}_{ij}^n=\frac{1}{2}\delta_t\left(\boldsymbol{v}_{ij}^n\right)^2, \tag{3.21}$$

$$\begin{aligned}\delta_x^2\rho_t\boldsymbol{u}_{ij}^n\cdot\rho_t\boldsymbol{v}_{ij}^n&=\delta_x^+\left(\rho_t\delta_x^-\boldsymbol{u}_{ij}^n\cdot\rho_t\boldsymbol{v}_{ij}^n\right)-\rho_t\delta_x^+\boldsymbol{u}_{i,j}^n\cdot\delta_t\boldsymbol{u}_{i+1,j}^n+\rho_t\delta_x^+\boldsymbol{u}_{i,j}^n\cdot\delta_t\boldsymbol{u}_{i,j}^n &(3.22)\\&=\delta_x^+\left(\rho_t\delta_x^-\boldsymbol{u}_{ij}^n\cdot\rho_t\boldsymbol{v}_{ij}^n\right)-\rho_t\delta_x^+\boldsymbol{u}_{i,j}^n\cdot\delta_x^+\delta_t\boldsymbol{u}_{i,j}^n &(3.23)\\&=\delta_x^+\left(\rho_t\delta_x^-\boldsymbol{u}_{ij}^n\cdot\rho_t\boldsymbol{v}_{ij}^n\right)-\frac{1}{2}\delta_t\left(\delta_x^+\boldsymbol{u}_{ij}^n\right)^2. &(3.24)\end{aligned}$$

Following similar analysis, we obtain

$$\delta_y^2\rho_t\boldsymbol{u}_{ij}^n\cdot\rho_t\boldsymbol{v}_{ij}^n=\delta_y^+\left(\rho_t\delta_y^-\boldsymbol{u}_{ij}^n\cdot\rho_t\boldsymbol{v}_{ij}^n\right)-\frac{1}{2}\delta_t\left(\delta_y^+\boldsymbol{u}_{ij}^n\right)^2. \tag{3.25}$$

Therefore, we can conclude from Eqs (3.19)–(3.25) that

$$\delta_t\Big(\frac{1}{2}(\boldsymbol{v}_{ij}^n)^2+\frac{1}{2}((\delta_x^+\boldsymbol{u}_{ij}^n)^2+(\delta_y^+\boldsymbol{u}_{ij}^n)^2)+(\boldsymbol{r}_{ij}^n)^2\Big)-\Big(\delta_x^+\left(\rho_t\delta_x^-\boldsymbol{u}_{ij}^n\cdot\rho_t\boldsymbol{v}_{ij}^n\right)+\delta_y^+\left(\rho_t\delta_y^-\boldsymbol{u}_{ij}^n\cdot\rho_t\boldsymbol{v}_{ij}^n\right)\Big)=-\beta(\rho_t\boldsymbol{v}_{ij}^n)^2\le 0. \tag{3.26}$$

The modified global energy dissipation law (3.17) can be obtained by combining the local energy dissipation law (3.16) and boundary conditions. Under homogeneous Dirichlet or periodic boundary conditions, by using the discrete summation-by-parts identities, it holds that

$$\sum_{i=1}^{N_x-1}\sum_{j=1}^{N_y-1}\left(\delta_x^+\left(\rho_t\delta_x^-\boldsymbol{u}_{i,j}^n\cdot\rho_t\boldsymbol{v}_{i,j}^n\right)+\delta_y^+\left(\rho_t\delta_y^-\boldsymbol{u}_{i,j}^n\cdot\rho_t\boldsymbol{v}_{i,j}^n\right)\right)=0.$$

Accordingly, summing Eq (3.16) over spatial grid points gives the global energy dissipation law

$$E^{n+1}-E^n=-\tau\beta\langle\rho_t\boldsymbol{v}^n,\rho_t\boldsymbol{v}^n\rangle\le 0,\quad n=0,1,\cdots,N-1. \tag{3.27}$$

Thus, we have completed the proof.

Remark 3.2. *We mention that when $\beta=0$, the fully-discrete* **LILED** *scheme* (3.13)–(3.15) *preserves the modified discrete local energy conservation law*

$$\delta_t\Big(\frac{1}{2}(\boldsymbol{v}_{ij}^n)^2+\frac{1}{2}((\delta_x^+\boldsymbol{u}_{ij}^n)^2+(\delta_y^+\boldsymbol{u}_{ij}^n)^2)+(\boldsymbol{r}_{ij}^n)^2\Big)-\left(\delta_x^+\left(\rho_t\delta_x^-\boldsymbol{u}_{ij}^n\cdot\rho_t\boldsymbol{v}_{ij}^n\right)+\delta_y^+\left(\rho_t\delta_y^-\boldsymbol{u}_{ij}^n\cdot\rho_t\boldsymbol{v}_{ij}^n\right)\right)\equiv 0.$$

Besides, the modified discrete global energy conservation law also holds under homogeneous Dirichlet or periodic boundary conditions, namely

$$E^N=E^{N-1}=\cdots=E^0.$$

3.3. A fast solver for the proposed scheme

In this section, we aim to design an efficient algorithm tailored to solve the proposed numerical scheme for improving computational performance, making it more practical and effective for real-world applications. First, one can observe that

$$\rho_t\boldsymbol{v}^n=\delta_t\boldsymbol{u}^n=\frac{\boldsymbol{u}^{n+1}-\boldsymbol{u}^n}{\tau}=\frac{2\rho_t\boldsymbol{u}^n-2\boldsymbol{u}^n}{\tau}, \tag{3.28}$$

and

$$\delta_t\boldsymbol{r}^n=\frac{\boldsymbol{r}^{n+1}-\boldsymbol{r}^n}{\tau}=\frac{2\rho_t\boldsymbol{r}^n-2\boldsymbol{r}^n}{\tau}. \tag{3.29}$$

According to Eq (3.15), we have

$$\rho_t\boldsymbol{r}^n=\boldsymbol{r}^n+\frac{1}{4}\mathcal{B}\left(\boldsymbol{u}^{n+1}-\boldsymbol{u}^n\right), \tag{3.30}$$

where

$$\mathcal{B}:=\operatorname{diag}\left(\varphi(\hat{\boldsymbol{u}}_{1,1}^n),\varphi(\hat{\boldsymbol{u}}_{2,1}^n),\cdots,\varphi(\hat{\boldsymbol{u}}_{N_x-1,1}^n),\cdots,\varphi(\hat{\boldsymbol{u}}_{1,N_y-1}^n),\cdots,\varphi(\hat{\boldsymbol{u}}_{N_x-1,N_y-1}^n)\right), \tag{3.31}$$

where $\varphi(z)=\frac{f(z)}{\sqrt{F(z)+C_0}}$. Substituting the above results into Eq (3.14) yields

$$\frac{\frac{2\boldsymbol{u}^{n+1}-2\boldsymbol{u}^n}{\tau}-2\boldsymbol{v}^n}{\tau}=\mathcal{D}\rho_t\boldsymbol{u}^n-\beta\frac{\boldsymbol{u}^{n+1}-\boldsymbol{u}^n}{\tau}-\mathcal{B}\Big(\boldsymbol{r}^n+\frac{1}{4}\mathcal{B}(\boldsymbol{u}^{n+1}-\boldsymbol{u}^n)\Big), \tag{3.32}$$

which can be further arranged as

$$\left(2I - \frac{\tau^2}{2}\mathcal{D} + \tau\beta I + \frac{\tau^2}{4}\mathcal{B}^2\right)\boldsymbol{u}^{n+1} = \mathcal{K}^n := \left(2I + \frac{\tau^2}{2}\mathcal{D} + \tau\beta I + \frac{\tau^2}{4}\mathcal{B}^2\right)\boldsymbol{u}^n + 2\tau\boldsymbol{v}^n - \tau^2\mathcal{B}\boldsymbol{r}^n, \tag{3.33}$$

where I is the $N_x \times N_y$ identity matrix and the matrix $\mathcal{D}$ represents the second-order central difference discretization $\delta_x^2 + \delta_y^2$. Denote

$$\mathcal{A} := 2I - \frac{\tau^2}{2}\mathcal{D} + \tau\beta I + \frac{\tau^2}{4}\mathcal{B}^2. \tag{3.34}$$

We can derive from Eq (3.34) that matrix $\mathcal{A}$ is a real symmetric and strictly diagonally dominant M-matrix, which means that it is positive definite and consequently invertible.

Next, we introduce a fast iterative solver to efficiently compute $\boldsymbol{u}^{n+1}$. To this end, we rewrite Eq (3.33) equivalently as

$$\left(2I - \frac{\tau^2}{2}\mathcal{D} + \tau\beta I\right)\boldsymbol{u}^{n+1} = \mathcal{K}^n - \frac{\tau^2}{4}\mathcal{B}^2\boldsymbol{u}^{n+1}. \tag{3.35}$$

Denote

$$\tilde{\mathcal{A}} := 2I - \frac{\tau^2}{2}\mathcal{D} + \tau\beta I. \tag{3.36}$$

In this way, we can use an iterative method to solve the linear system (3.35), namely,

$$\tilde{\mathcal{A}}\boldsymbol{u}^{n+1(s+1)} = \mathcal{K}^n - \frac{\tau^2}{4}\mathcal{B}^2\boldsymbol{u}^{n+1(s)}. \tag{3.37}$$

The initial value for the iterative process can be set as $\boldsymbol{u}^{n+1(0)} = \boldsymbol{u}^n$. The differential matrix $\mathcal{D}$ can be decomposed as $\mathcal{D} := \mathcal{F}^{-1}\Lambda\mathcal{F}$, where $\mathcal{F}$ and $\mathcal{F}^{-1}$ are the discrete Fourier transform matrix and its inverse matrix, respectively. The diagonal matrix Λ contains the eigenvalues of $\mathcal{D}$ as its entries. Using this decomposition, the coefficient matrix $\tilde{\mathcal{A}}$ can be rewritten as

$$\tilde{\mathcal{A}} = \mathcal{F}^{-1}\mathbb{D}\mathcal{F}, \tag{3.38}$$

where

$$\mathbb{D} = 2I - \frac{\tau^2}{2}\Lambda + \tau\beta I. \tag{3.39}$$

Moreover, the inverse matrix of $\tilde{\mathcal{A}}$ satisfies

$$\tilde{\mathcal{A}}^{-1} = \mathcal{F}^{-1}\mathbb{D}^{-1}\mathcal{F}. \tag{3.40}$$

The computational cost of $\tilde{\mathcal{A}}^{-1}$ is negative since $\mathbb{D}$ is a diagonal matrix. Therefore, $\boldsymbol{u}^{n+1(s+1)}$ can be efficiently determined by Eq (3.37). The iteration process stops once the difference between two successive iteration values is less than a specified, very small threshold. Consequently, we set $\boldsymbol{u}^{n+1} = \boldsymbol{u}^{n+1(s+1)}$, then we further obtain $\boldsymbol{v}^{n+1}$ and $\boldsymbol{r}^{n+1}$ by Eqs (3.13) and (3.15), respectively.

4. Unique solvability and convergence of the LILED scheme

In this section, we explore the unique solvability and convergence of the **LILED** scheme presented in Eqs (3.13)–(3.15).

4.1. Unique solvability

Building upon the discussions in subsection 3.3, we promptly reach the following conclusion.

Theorem 4.1. The developed **LILED** scheme (3.13)–(3.15) has a unique solution.

Proof. Since $\mathcal{A}$ is invertible in subsection 3.3, multiplying Eq (3.33) with $\mathcal{A}^{-1}$, we can obtain

$$\boldsymbol{u}^{n+1} = \mathcal{A}^{-1}\mathcal{K}^n.$$

Thus, we have completed proof.

4.2. Convergence analysis

Through the application of the energy method, in this subsection, we formulate an optimal error estimate for the proposed scheme. First, we revisit some initial findings that hold a crucial significance in error analysis.

Lemma 4.1. *(Grönwall inequality [49]). Suppose that the discrete function* $\{u^n | n = 1, 2, \cdots, N; N\tau = T\}$ *is nonnegative and satisfies the inequality*

$$u^n \le \widetilde{A} + \tau \sum_{k=1}^{n} \widetilde{B}_k u^k,$$

where $\widetilde{A}$ *and* $\widetilde{B}_k$ $(k = 1, 2, \cdots, N)$ *are nonnegative constants. Then*

$$\max_{1\le n\le N} |u^n| \le \widetilde{A} \exp\left(2\tau \sum_{k=1}^{N} \widetilde{B}_k\right),$$

where τ *is sufficiently small such that* $\tau(\max\limits_{k=1,2,\cdots,N} \widetilde{B}_k) \le \frac{1}{2}$.

Lemma 4.2. *Based on the fact that the function* $f(u)$ *satisfies the Lipschitz condition, namely* $|\partial_u f(u)|$ *is bounded, then we further have*

$$|\varphi(u)| \lesssim C, \qquad |\partial_u \varphi(u)| \lesssim C,$$

here and in the follow-up of the article, C denotes a constant that may vary depending on the context.

Assuming (u, v, r) is the exact solution of the equivalent systems (2.2)–(2.4), then $(u_{ij}^n, v_{ij}^n, r_{ij}^n)$ satisfies following fully-discrete equations

$$\delta_t u_{ij}^n = \rho_t v_{ij}^n + (\theta_1^n)_{ij}, \tag{4.1}$$

$$\delta_t v_{ij}^n = \delta_x^2 \rho_t u_{ij}^n + \delta_y^2 \rho_t u_{ij}^n - \beta \rho_t v_{ij}^n - \frac{f(\hat{u}_{ij}^n)}{\sqrt{F(\hat{u}_{ij}^n) + C_0}} \rho_t r_{ij}^n + (\theta_2^n)_{ij}, \tag{4.2}$$

$$\delta_t r_{ij}^n = \frac{1}{2} \frac{f(\hat{u}_{ij}^n)}{\sqrt{F(\hat{u}_{ij}^n) + C_0}} \rho_t v_{ij}^n + (\theta_3^n)_{ij}. \tag{4.3}$$

Assuming $u \in C^4\left([0,T],L^2(\Omega)\right), v \in C^3\left([0,T],L^2(\Omega)\right)$, and $r \in C^3\left([0,T],L^2(\Omega)\right)$, then using the Taylor formula, we can obtain

$$|(\theta_k^n)_{ij}| \le C(h^2+\tau^2) \quad \text{for} \quad n \ge 1, \quad |(\theta_k^0)_{ij}| \le C(h^2+\tau), \quad k=1,2,3, \tag{4.4}$$

$$|\delta_x(\theta_1^n)_{ij}| + |\delta_y(\theta_1^n)_{ij}| \le C(h^2+\tau^2). \tag{4.5}$$

Define the following error vector functions

$$\varepsilon_z^n = z^n - \boldsymbol{z}^n, \quad z=u,v,r, \quad \text{for} \quad 0 \le n \le N, \quad \text{with} \quad e_z^0 = \mathbf{0}. \tag{4.6}$$

Then subtracting Eqs (3.13)–(3.15) from Eqs (4.1)–(4.3), we obtain error equations

$$\delta_t \varepsilon_u^n = \rho_t \varepsilon_v^n + \theta_1^n, \tag{4.7}$$

$$\delta_t \varepsilon_v^n = \delta_x^2 \rho_t \varepsilon_u^n + \delta_y^2 \rho_t \varepsilon_u^n - \beta \rho_t \varepsilon_v^n - \varphi(\hat{u}^n)\rho_t r^n + \varphi(\hat{\boldsymbol{u}}^n)\rho_t \boldsymbol{r}^n + \theta_2^n, \tag{4.8}$$

$$\delta_t \varepsilon_r^n = \frac{1}{2}\Big(\varphi(\hat{u}^n)\rho_t v^n - \varphi(\hat{\boldsymbol{u}}^n)\rho_t \boldsymbol{v}^n\Big) + \theta_3^n. \tag{4.9}$$

Theorem 4.2. *Assuming $u \in C^4\left([0,T],L^2(\Omega)\right), v \in C^3\left([0,T],L^2(\Omega)\right)$, and $r \in C^3\left([0,T],L^2(\Omega)\right)$, $\boldsymbol{u}^n, \boldsymbol{v}^n, \boldsymbol{r}^n$, are the numerical solutions of the proposed* **LILED** *scheme* (3.13)–(3.15)*, respectively. Then for sufficiently small τ, we get*

$$\|\boldsymbol{u}^n - u^n\|_{H_h^1} + \|\boldsymbol{v}^n - v^n\| + \|\boldsymbol{r}^n - r^n\| \le C(h^2+\tau^2). \tag{4.10}$$

Proof. We first estimate $\|\varepsilon_u^1\|_{H_h^1}$, $\|\varepsilon_v^1\|$ and $\|\varepsilon_r^1\|$. To this end, computing discrete inner product of Eqs (4.7)–(4.9) for $n=0$ with ε_u^1, ε_v^1, and ε_r^1, respectively, we have

$$\|\varepsilon_u^1\|^2 = \frac{\tau}{2}\langle \varepsilon_v^1, \varepsilon_u^1\rangle + \tau\langle \theta_1^0, \varepsilon_u^1\rangle, \tag{4.11}$$

$$\|\varepsilon_v^1\|^2 + \|\delta_x^2\varepsilon_u^1\|^2 + \|\delta_y^2\varepsilon_u^1\|^2 = -\frac{\beta\tau}{2}\|\varepsilon_v^1\|^2 - \tau\Big\langle \varphi(\hat{\boldsymbol{u}}^1)\varepsilon_r^1, \varepsilon_v^1\Big\rangle + \frac{\tau}{2}\Big\langle \theta_2^0, \varepsilon_v^1\Big\rangle - 2\tau\Big\langle \delta_x^2\varepsilon_u^1 + \delta_y^2\varepsilon_u^1, \theta_1^0\Big\rangle, \tag{4.12}$$

$$\|\varepsilon_r^1\|^2 = \frac{\tau}{4}\Big\langle (\varphi(\hat{\boldsymbol{u}}^0)\cdot \varepsilon_v^1, \varepsilon_r^1\Big\rangle + \tau\langle \theta_3^0, \varepsilon_r^1\rangle. \tag{4.13}$$

Through direct calculations, we can derive from Eqs (4.11)–(4.13) that

$$\|\varepsilon_u^1\|_{H_h^1} + \|\varepsilon_v^1\| + \|\varepsilon_r^1\| \le C\tau(\|\varepsilon_u^1\|_{H_h^1} + \|\varepsilon_v^1\| + \|\varepsilon_r^1\|) + C\tau\left(h^2+\tau^1\right). \tag{4.14}$$

Therefore, when $C\tau \le \frac{1}{2}$, it further indicates

$$\|\varepsilon_u^1\|_{H_h^1} + \|\varepsilon_v^1\| + \|\varepsilon_r^1\| \le C\left(h^2+\tau^2\right). \tag{4.15}$$

Subsequently, the error estimate Eq (4.10) is valid for $n=1$.

Now taking discrete inner product of Eqs (4.7)–(4.9) for $n>1$ with $\rho_t\varepsilon_u^n$, $\rho_t\varepsilon_v^n$, and $\rho_t\varepsilon_r^n$, respectively, we can obtain

$$\frac{1}{2}\delta_t\|\varepsilon_u^n\|^2 = \vartheta_1^n, \tag{4.16}$$

$$\frac{1}{2}\delta_t\|\varepsilon_v^n\|^2+\frac{1}{2}\delta_t\|\delta_x^2\varepsilon_u^n\|^2+\frac{1}{2}\delta_t\|\delta_y^2\varepsilon_u^n\|^2=-\beta\|\rho_t\varepsilon_v^n\|^2+\vartheta_2^n, \tag{4.17}$$

$$\frac{1}{2}\delta_t\|\varepsilon_r^n\|^2=\vartheta_3^n, \tag{4.18}$$

where

$$\vartheta_1^n=\langle\rho_t\varepsilon_v^n,\rho_t\varepsilon_u^n\rangle+\langle\theta_1^n,\rho_t\varepsilon_u^n\rangle, \tag{4.19}$$

$$\vartheta_2^n=-\Big\langle(\varphi(\hat{u}^n)-\varphi(\hat{\boldsymbol{u}}^n))\cdot\rho_t r^n+\varphi(\hat{\boldsymbol{u}}^n)\cdot\rho_t\varepsilon_r^n,\rho_t\varepsilon_v^n\Big\rangle+\Big\langle\theta_2^n,\rho_t\varepsilon_v^n\Big\rangle-\Big\langle\delta_x^2\rho_t\varepsilon_u^n+\delta_y^2\rho_t\varepsilon_u^n,\theta_1^n\Big\rangle, \tag{4.20}$$

$$\vartheta_3^n=\frac{1}{2}\Big\langle(\varphi(\hat{u}^n)-\varphi(\hat{\boldsymbol{u}}^n))\cdot\rho_t v^n+\varphi(\hat{\boldsymbol{u}}^n)\cdot\rho_t\varepsilon_v^n,\rho_t\varepsilon_r^n\Big\rangle+\langle\theta_3^n,\rho_t\varepsilon_r^n\rangle. \tag{4.21}$$

Applying Lemma 4.2, along with the Hölder inequality and the Cauchy mean value theorem, we derive

$$\|(\varphi(\hat{u}^n)-\varphi(\hat{\boldsymbol{u}}^n))\cdot\rho_t r^n\|\le\|\rho_t r^n\|_\infty\|\varphi(\hat{u}^n)-\varphi(\hat{\boldsymbol{u}}^n)\|\le C\|\hat{\varepsilon}_u^n\|\le C(\|\varepsilon_u^n\|+\varepsilon_u^{n-1}\|), \tag{4.22}$$

and

$$\|(\varphi(\hat{u}^n)-\varphi(\hat{\boldsymbol{u}}^n))\cdot\rho_t v^n\|\le\|\rho_t v^n\|_\infty\|\varphi(\hat{u}^n)-\varphi(\hat{\boldsymbol{u}}^n)\|\le C\|\hat{\varepsilon}_u^n\|\le C(\|\varepsilon_u^n\|+\varepsilon_u^{n-1}\|). \tag{4.23}$$

A similar discussion can yield

$$\|\varphi(\hat{\boldsymbol{u}}^n)\cdot\rho_t\varepsilon_v^n\|\le C(\|\varepsilon_v^n\|+\varepsilon_v^{n+1}\|), \tag{4.24}$$

and

$$\|\varphi(\hat{\boldsymbol{u}}^n)\cdot\rho_t\varepsilon_r^n\|\le C(\|\varepsilon_r^n\|+\varepsilon_r^{n+1}\|). \tag{4.25}$$

These results with Eqs (4.19)–(4.21) indicate that

$$\vartheta_1^n\le C(\|\varepsilon_u^n\|^2+\|\varepsilon_v^n\|^2+\|\varepsilon_u^{n+1}\|^2+\|\varepsilon_v^{n+1}\|^2+(h^2+\tau^2)^2), \tag{4.26}$$

$$\vartheta_2^n\le C\Big(\|\varepsilon_u^{n-1}\|^2+\|\varepsilon_u^n\|_{H_h^1}^2+\|\varepsilon_u^{n+1}\|_{H_h^1}^2+\|\varepsilon_v^n\|^2+\|\varepsilon_v^{n+1}\|^2+\|\varepsilon_r^n\|^2+\|\varepsilon_r^{n+1}\|^2+(h^2+\tau^2)^2\Big), \tag{4.27}$$

$$\vartheta_3^n\le C\Big(\|\varepsilon_u^{n-1}\|^2+\|\varepsilon_u^n\|^2+\|\varepsilon_v^n\|^2+\|\varepsilon_v^{n+1}\|^2+\|\varepsilon_r^n\|^2+\|\varepsilon_r^{n+1}\|^2+(h^2+\tau^2)^2\Big). \tag{4.28}$$

For convenience of convergence analysis, we further define χ^n as

$$\chi^n:=\|\varepsilon_u^n\|_{H_h^1}^2+\|\varepsilon_v^n\|^2+\|\varepsilon_r^n\|^2. \tag{4.29}$$

By combining Eqs (4.16)–(4.18), and taking into account Eqs (4.26)–(4.28), we obtain

$$\begin{aligned}&\delta_t\Big(\|\varepsilon_u^n\|^2+\|\delta_x\varepsilon_u^n\|^2+\|\delta_y\varepsilon_u^n\|^2+\|\varepsilon_v^n\|^2+\|\varepsilon_r^n\|^2\Big)\\&\quad\le C\Big(\|\varepsilon_u^{n-1}\|^2+\|\varepsilon_u^n\|_{H_h^1}^2+\|\varepsilon_u^{n+1}\|_{H_h^1}^2+\|\varepsilon_v^n\|^2+\|\varepsilon_v^{n+1}\|^2+\|\varepsilon_r^n\|^2+\|\varepsilon_r^{n+1}\|^2\Big)+C\left(h^2+\tau^2\right)^2.\end{aligned} \tag{4.30}$$

This inequality can be equivalently expressed as

$$\chi^{n+1} - \chi^n \leq C\tau\left(\chi^{n+1} + \chi^n\right) + C\tau\|\varepsilon_u^{n-1}\|^2 + C\tau\left(h^2 + \tau^2\right)^2. \tag{4.31}$$

By summing Eq (4.31) from 2 to n, we derive from Eqs (4.15) and (4.31) that

$$\begin{aligned}\chi^n &\leq \chi^1 + C\tau\sum_{l=1}^{n}\chi^l + C\tau\|\varepsilon_u^0\|^2 + C\left(h^2 + \tau^2\right)^2 \\ &\leq C\tau\sum_{l=1}^{n}\chi^l + C\left(h^2 + \tau^2\right)^2.\end{aligned} \tag{4.32}$$

Applying the Grönwall inequality as described in Lemma 4.1 to system (4.32), it holds that

$$\|\varepsilon_u^n\|_{H_h^1}^2 + \|\varepsilon_v^n\|^2 + \|\varepsilon_r^n\|^2 \leq C\mathrm{e}^{2C\tau}\left(h^2 + \tau^2\right)^2, \tag{4.33}$$

which further implies that

$$\|\varepsilon_u^n\|_{H_h^1} + \|\varepsilon_v^n\| + \|\varepsilon_r^n\| \leq C\left(h^2 + \tau^2\right), \quad n = 1, 2, \cdots, N, \tag{4.34}$$

where time step τ is taken sufficiently small such that $C\tau \leq \frac{1}{2}$.

Thus, we have completed proof.

Remark 4.1. *It should be particularly noted that local energy dissipation law is an inherent property of the nonlinear wave equation, whose validity is independent of boundary conditions. However, in the construction of fully discrete numerical schemes, it is necessary to select appropriate spatial discretization methods according to different boundary conditions, such as the finite element method, finite difference method, and pseudospectral method. Despite the differences in discretization methods for spatial direction, consistent theoretical results can still be obtained, and the numerical example results further verify the correctness of the theoretical analysis.*

5. Numerical examples

In this section, we present numerical results to demonstrate the energy stability, efficiency, and accuracy of the proposed method.

Example 5.1. *We begin by testing the accuracy of the proposed scheme for the one-dimensional nonlinear Sine-Gordon model*

$$u_{tt} - \Delta u + \beta u_t + \sin(u) = 0, \quad x \in \Omega, \tag{5.1}$$

with the initial conditions $u(x, 0) = 0$ *and* $v(x, 0) = \frac{4}{\gamma}sech\left(\frac{x}{\gamma}\right)$ *for* $x \in \Omega = (-10, 10)$.

We set $\beta = 0$ and apply periodic boundary condition. The analytical solution is given by

$$u(x, t) = 4\tan^{-1}\left[\psi(t; \gamma)\mathrm{sech}\left(\frac{x}{\gamma}\right)\right],$$

where the function $\psi(t; \gamma)$ takes different forms based on the value of γ, as follows

- For $\gamma > 1$:

$$\psi(t;\gamma) = \frac{\sin(\gamma^{-1}\sqrt{\gamma^2 - 1}t)}{\sqrt{\gamma^2 - 1}},$$

- For $\gamma = 1$:

$$\psi(t;\gamma) = t,$$

- For $0 < \gamma < 1$:

$$\psi(t;\gamma) = \frac{\sinh(\gamma^{-1}\sqrt{1 - \gamma^2}t)}{\sqrt{1 - \gamma^2}}.$$

To evaluate the performance of the newly developed scheme, we compare it with local structure-preserving schemes of the same order in both space and time directions.

- **SM**: The symplectic midpoint finite difference scheme as described in [50, 51].
- **MSB**: The multi-symplectic box scheme, detailed in [52].
- **EP**: The energy-dissipation finite difference scheme proposed in [45].

First, we select $\beta = 0$ and $\gamma = 1.5$ to test the accuracy of these schemes. Table 1 summarizes the numerical errors and convergence orders of four schemes, **LILED**, **EP**, **MSB**, and **SM**, at $T = 1$. It presents L^2-errors and L^∞-errors along with their corresponding convergence orders. For each scheme, the errors decrease as the grid resolution (h) and time step (τ) are refined, indicating that these schemes exhibit second-order convergence in temporal and spatial directions. Among the schemes, **MSB** demonstrates the highest convergence orders for both L^2-errors and L^∞-errors, closely followed by **SM**, which also performs well in terms of accuracy. The **LILED** and **EP** schemes achieve reliable second-order convergence, while showing slightly lower error reductions compared to **MSB**. Figure 1 compares the CPU time for four schemes using different mesh sizes ($h = 1/10, 1/20, 1/40$) and a fixed time step $\tau = 0.01$. The CPU time is shown on a logarithmic scale to highlight the differences in computational efficiency. The results indicate that our method has higher computational efficiency than other schemes.

Table 1. The numerical errors and convergence orders of four schemes at $T = 1$.

Scheme	(h, τ)	L^2-error	order	L^∞-error	order
	$(\frac{1}{10}, \frac{1}{10})$	2.1692×10^{-2}	-	1.4317×10^{-2}	-
LILED	$(\frac{1}{20}, \frac{1}{20})$	5.5039×10^{-3}	1.9786	3.6306×10^{-3}	1.9794
	$(\frac{1}{40}, \frac{1}{40})$	1.3830×10^{-3}	1.9926	9.1158×10^{-4}	1.9937
	$(\frac{1}{10}, \frac{1}{10})$	1.8237×10^{-3}	-	1.1171×10^{-3}	-
EP	$(\frac{1}{20}, \frac{1}{20})$	4.5729×10^{-4}	1.9956	2.8188×10^{-4}	1.9866
	$(\frac{1}{40}, \frac{1}{40})$	1.1442×10^{-4}	1.9987	7.0588×10^{-5}	1.9975
	$(\frac{1}{10}, \frac{1}{10})$	3.3718×10^{-3}	-	2.9440×10^{-3}	-
MSB	$(\frac{1}{20}, \frac{1}{20})$	8.4184×10^{-4}	2.0019	7.3485×10^{-4}	2.0023
	$(\frac{1}{40}, \frac{1}{40})$	2.0962×10^{-4}	2.0004	1.8261×10^{-4}	2.0006
	$(\frac{1}{10}, \frac{1}{10})$	2.3650×10^{-3}	-	1.4000×10^{-3}	-
SM	$(\frac{1}{20}, \frac{1}{20})$	5.9209×10^{-4}	1.9979	3.5235×10^{-4}	1.9903
	$(\frac{1}{40}, \frac{1}{40})$	1.4809×10^{-4}	1.9993	8.8245×10^{-5}	1.9974

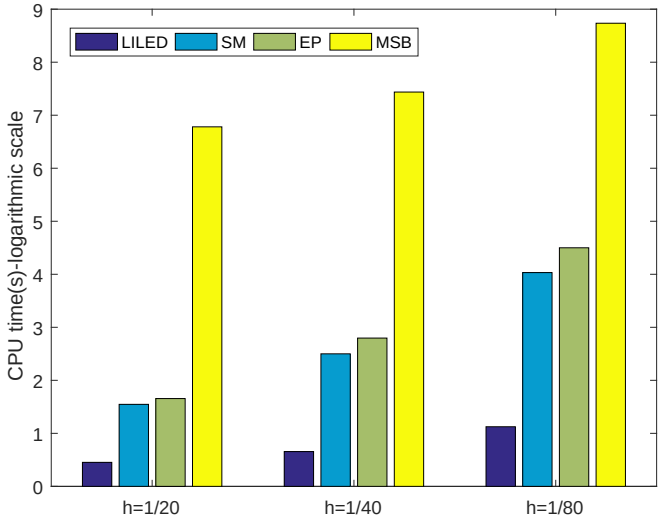

Figure 1. CPU time of these schemes with different mesh sizes for $T = 1$ under $\tau = 0.01$.

Figure 2 shows the energy evolution process for the proposed scheme with $h = 0.1$, $\tau = 0.01$, and $T = 10$ under two conditions: On the left for a conservative system with $\beta = 0$, and on the right for a dissipative system with $\beta = 2$. The plot shows the discrete Hamiltonian energy (1.10) as well as the **LILED** energy (3.18) over time. In the left plot (conservative system), the Hamiltonian energies oscillate, and the **LILED** energy remain nearly constant, indicating the conservation of modified **LILED** energy. In contrast, the right plot (dissipative system) shows a steady decrease in the energies as time progresses, reflecting the energy dissipation due to the damping effect of $\beta = 2$. In conclusion, the proposed **LILED** scheme is an efficiently structure-preserving method to solve the nonlinear wave

equation, and has advantages in accuracy, efficiency, and the preservation of energy structure. Its ability to balance computational cost with numerical stability makes it especially well-suited for long-term simulations.

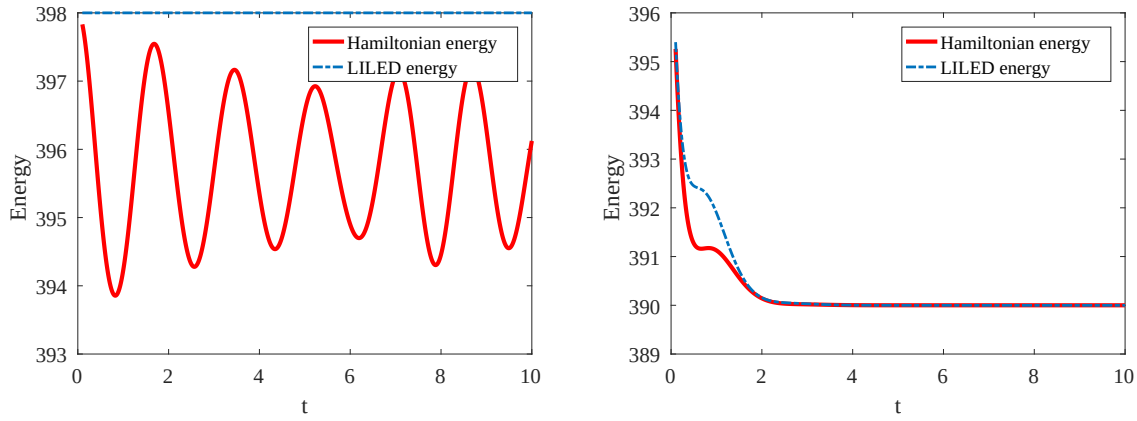

Figure 2. The energy evolution process for the proposed scheme with $h = 0.1, \tau = 0.01$ at $T = 10$ for $\beta = 0$ (left: conservative system), and $\beta = 2$ (right: dissipative system).

Example 5.2. *Consider the two-dimensional generalized wave equation with the initial conditions*

$$u(x, y, 0) = 4 \tan^{-1}\left[\exp\left(\frac{4 - \sqrt{(x+3)^2 + (y+7)^2}}{0.436}\right)\right],$$
$$v(x, y, 0) = \frac{4.13}{\cosh\left(\frac{4 - \sqrt{(x+3)^2+(y+7)^2}}{0.436}\right)}, \qquad (x, y) \in (-30, 10) \times (-21, 7).$$

In Figure 3, we present the **LILED** energy evolution process of the proposed scheme for different values of β. The energy, shown on the vertical axis, decreases over time, represented by three curves for $\beta = 7$ (red), $\beta = 3$ (blue dashed), and $\beta = 0.5$ (blue dotted). The horizontal axis represents time t, ranging from 0 to 40. The spatial grid size $h = 0.1$, time step $\tau = 0.01$, and total time $T = 40$ are set for the experiment. Initially, the energy is high and gradually decays over time. The differing rates of energy decay for different values of β are illustrated. Figure 4 describes numerical solutions obtained using the proposed scheme with a grid size of $N = 256$ and time step $\tau = 0.1$. The plot displays the isosurfaces of the solution for three values of β (specifically, $\beta = 0.5$, $\beta = 3$, and $\beta = 7$) at $t = 1, 3, 4$, and 6. The shapes of the isosurfaces evolve over time, reflecting the dynamic behavior of the modeled system. This sequence of visualizations demonstrates how the solution changes with respect to parameter β and time. The different behaviors at each value of β provide insight into the spatial distribution and temporal evolution of the quantities under study.

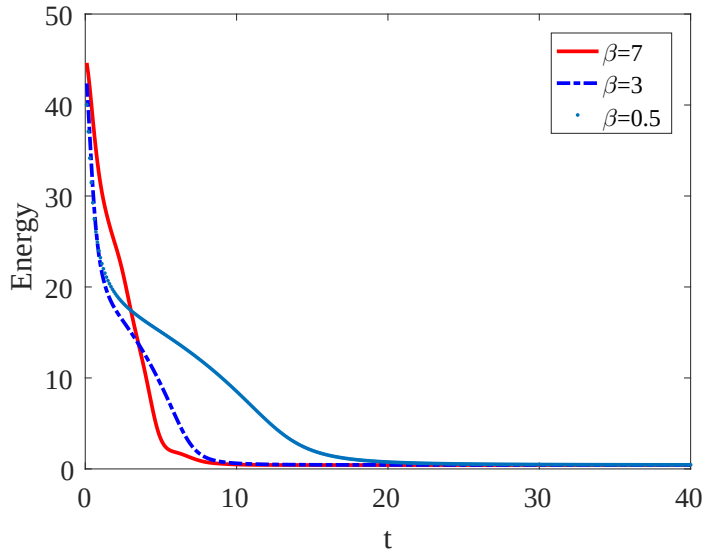

Figure 3. The **LILED** energy evolution process for the proposed scheme with $h = 0.1, \tau = 0.01$ at $T = 40$ for $\beta = 0.5,\ 3,\ 7$.

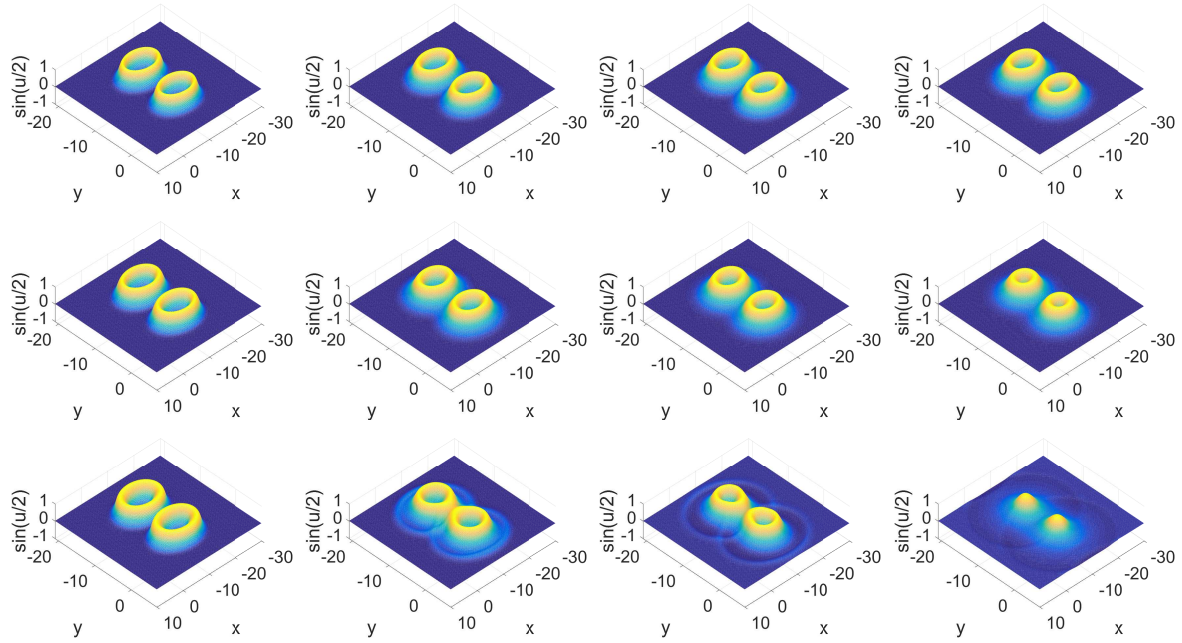

Figure 4. Numerical solutions obtained by the **LILED** scheme with $N = 256$ and $\tau = 0.1$, the isosurfaces of $\beta = 0.5$ (top), $\beta = 3$ (middle), and $\beta = 7$ (down) at $t = 1, 3, 4, 6$.

Example 5.3. *Consider the two-dimensional sine-Gordon equation with homogeneous Neumann boundary condition* ($\nabla u \cdot \mathbf{n} = 0$ *along the boundary of* Ω*), and the initial conditions are set as*

$$u(x,y,0) = 4\tan^{-1}\Big[\exp\Big(\frac{4-\sqrt{(x+3)^2+(y+3)^2}}{0.436}\Big)\Big] + 4\tan^{-1}\Big[\exp\Big(\frac{4-\sqrt{(x+3)^2+(y+17)^2}}{0.436}\Big)\Big]$$

$$+4\tan^{-1}\Big[\exp\Big(\frac{4-\sqrt{(x+17)^2+(y+3)^2}}{0.436}\Big)\Big]+4\tan^{-1}\Big[\exp\Big(\frac{4-\sqrt{(x+17)^2+(y+17)^2}}{0.436}\Big)\Big],$$

$$\begin{aligned} v(x,y,0) =& 4.13sech\Big(\frac{4-\sqrt{(x+3)^2+(y+3)^2}}{0.436}\Big)+4.13sech\Big(\frac{4-\sqrt{(x+3)^2+(y+17)^2}}{0.436}\Big)\\ &+4.13sech\Big(\frac{4-\sqrt{(x+17)^2+(y+3)^2}}{0.436}\Big)+4.13sech\Big(\frac{4-\sqrt{(x+17)^2+(y+17)^2}}{0.436}\Big). \end{aligned}$$

Here, the computational region is selected as $\Omega = (-30, 10) \times (-30, 10)$. Through mathematical derivation, we can find that the local energy dissipation law (1.5) and global energy dissipation law (1.9) hold for the nonlinear wave Eq (1.1) under the homogeneous Neumann boundary condition. The second-order central difference scheme based on the cell-centered grid is adopted for spatial discretization [53]. The evolution of the **LILED** energy over time is plotted on the left side of Figure 5, which is consistent with the theoretical analysis obtained in Theorem 3.2. Finally, the surface of numerical solution at $t = 2$ in terms of $\sin(\frac{u}{2})$ is presented on the right side of Figure 5.

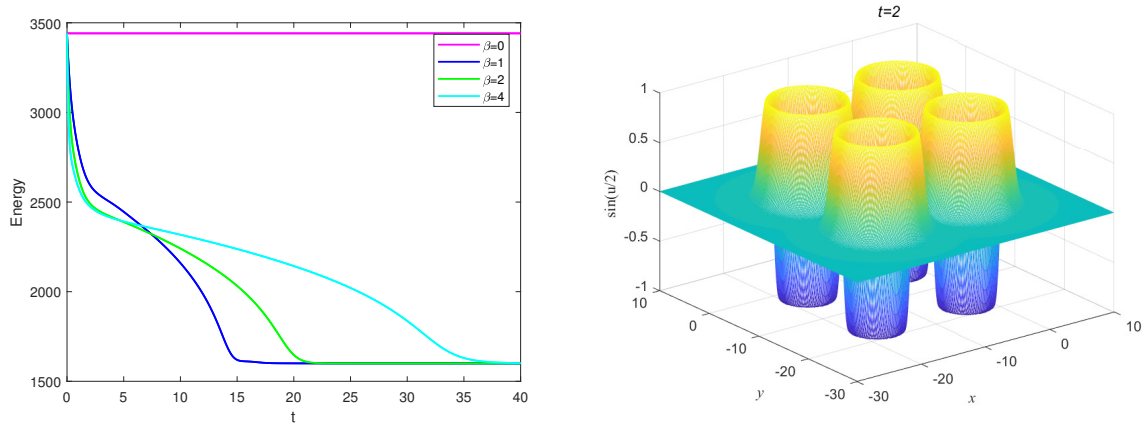

Figure 5. The **LILED** energy evolution process for different β (left) and surface plot of numerical solution at time $t = 2$ for $\beta = 2$ (right) with $h = 0.2$, and $\tau = 0.01$.

6. Conclusions

In this paper, we present a linearly implicit local structure-preserving scheme for solving the generalized nonlinear wave equation using the energy quadratization method. The scheme is linear, second-order, and computationally efficient, while ensuring the preservation of local and global energy dissipation laws. We provide detailed proofs of its energy stability properties and discuss its unique solvability. A thorough error analysis is also carried out. Numerical examples are included to demonstrate the scheme's accuracy, energy stability, and overall effectiveness.

Use of AI tools declaration

The authors declare they have not used Artificial Intelligence (AI) tools in the creation of this article.

Acknowledgments

This work is supported by the National Natural Science Foundation of China (12501536, 12201071), Scientific Research Fund of Hunan Provincial Education Department (23A0602).

Conflict of interest

The authors declare there is no conflict of interest.

Author contributions

All authors contributed equally to this work. Yulian Yi and Yuchen Yin were responsible for the theoretical analysis and the construction of the numerical scheme. Mingfa Fei conceived the original idea and supervised the project.

References

1. D. Hu, Fully decoupled and high-order linearly implicit energy-preserving RK-GSAV methods for the coupled nonlinear wave equation, *J. Comput. Appl. Math.*, **445** (2024), 115836. https://doi.org/10.1016/j.cam.2024.115836
2. L. Liu, C. Li, Coupled sine-Gordon systems in DNA dynamics, *Adv. Math. Phys.*, **2018** (2018), 4676281. https://doi.org/10.1155/2018/4676281
3. S. Joseph, New traveling wave exact solutions to the coupled Klein-Gordon system of equations, *Partial Differ. Equations Appl. Math.*, **5** (2022), 100208. https://doi.org/10.1016/j.padiff.2021.100208
4. B. Josephson, Supercurrents through barriers, *Adv. Phys.*, **14** (2006), 419–451. https://doi.org/10.1080/00018736500101091
5. Q. Sheng, A. Khaliq, D. Voss, Numerical simulation of two-dimensional sine-Gordon solitons via a split cosine scheme, *Math. Comput. Simul.*, **68** (2005), 355–373. https://doi.org/10.1016/j.matcom.2005.02.017
6. S. Dong, Z. Wyatt, Stability of a coupled wave-Klein-Gordon system with quadratic nonlinearities, *J. Differ. Equations*, **269** (2020), 7470–7497. https://doi.org/10.1016/j.jde.2020.05.019
7. M. Grote, A. Schneebeli, D. Schötzau, Discontinuous Galerkin finite element method for the wave equation, *SIAM J. Numer. Anal.*, **44** (2006), 2408–2431. https://doi.org/10.1137/05063194X
8. G. Richter, An explicit finite element method for the wave equation, *Appl. Numer. Math.*, **16** (1994), 65–80. https://doi.org/10.1016/0168-9274(94)00048-4
9. A. Pleshkevich, D. Vishnevskiy, V. Lisitsa, Sixth-order accurate pseudo-spectral method for solving one-way wave equation, *Appl. Math. Comput.*, **359** (2019), 34–51. https://doi.org/10.1016/j.amc.2019.04.029
10. K. Djidjeli, W. Price, E. Twizell, Q. Cao, A linearized implicit pseudo-spectral method for some model equations: The regularized long wave equations, *Commun. Numer. Methods Eng.*, **19** (2003), 847–863. https://doi.org/10.1002/cnm.635

11. Y. Zhao, X. Gu, A low-rank algorithm for strongly damped wave equations with visco-elastic damping and mass terms, *ESAIM: Math. Model. Numer. Anal.*, **59** (2025), 1747–1761. https://doi.org/10.1051/m2an/2025042
12. W. Luo, X. Gu, B. Carpentieri, J. Guo, A Bernoulli-barycentric rational matrix collocation method with preconditioning for a class of evolutionary PDEs, *Numer. Linear Algebra Appl.*, **32** (2025), e70007. https://doi.org/10.1002/nla.70007
13. Y. Chen, H. Zhu, S. Song, Multi-symplectic splitting method for the coupled nonlinear Schrödinger equation, *Comput. Phys. Commun.*, **181** (2011), 1231–1241. https://doi.org/10.1016/j.cpc.2010.03.009
14. C. Jiang, J. Sun, H. Li, Y. Wang, A fourth-order AVF method for the numerical integration of sine-Gordon equation, *Appl. Math. Comput.*, **313** (2017), 144–158. https://doi.org/10.1016/j.amc.2017.05.055
15. B. Leimkuhler, S. Reich, *Simulating Hamiltonian Dynamics*, Cambridge university press, Cambridge, 2004. https://doi.org/10.1016/j.amc.2017.05.055
16. Y. Li, X. Wu, Exponential integrators preserving first integrals or Lyapunov functions for conservative or dissipative systems, *SIAM J. Sci. Comput.*, **38** (2016), A1876–A1895. https://doi.org/10.1137/15M1023257
17. L. Brugnano, C. Zhang, D. Li, A class of energy-conserving Hamiltonian boundary value methods for nonlinear Schrödinger equation with wave operator, *Commun. Nonlinear Sci. Numer. Simul.*, **60** (2018), 33–49. https://doi.org/10.1016/j.cnsns.2017.12.018
18. K. Feng, M. Qin, *Symplectic Geometric Algorithms for Hamiltonian Systems*, Springer, Berlin, 2010. Available from: https://link.springer.com/book/10.1007/978-3-642-01777-3.
19. W. Bao, X. Zhao, A uniformly accurate (UA) multiscale time integrator Fourier pseudospectral method for the Klein-Gordon-Schrödinger equations in the nonrelativistic limit regime, *Numer. Math.*, **135** (2007), 833–873. https://doi.org/10.1007/s00211-016-0818-x
20. Y. Gong, Q. Hong, Q. Wang, Supplementary variable method for thermodynamically consistent partial differential equations, *Comput. Methods Appl. Mech. Eng.*, **381** (2021), 113746. https://doi.org/10.1016/j.cma.2021.113746
21. F. Yin, Z. Xu, Y. Fu, Novel high-order explicit energy-preserving schemes for NLS-type equations based on the Lie-group method, *Math. Comput. Simul.*, **225** (2024), 570–585. https://doi.org/10.1016/j.matcom.2024.05.029
22. X. Li, L. Zhang, High-order conservative energy quadratization schemes for the Klein-Gordon-Schrödinger equation, *Adv. Comput. Math.*, **48** (2022), 41. https://doi.org/10.1007/s10444-022-09962-2
23. Z. Zhang, J. Shen, Efficient structure preserving schemes for the Klein-Gordon-Schrödinger equations, *J. Sci. Comput.*, **89** (2021), 47. https://doi.org/10.1007/s10915-021-01649-y
24. Q. Hong, J. Li, Q. Wang. Supplementary variable method for structure-preserving approximations to partial differential equations with deduced equations, *Appl. Math. Lett.*, **110** (2020), 106576. https://doi.org/10.1016/j.aml.2020.106576

25. E. Hairer, C. Lubich, G. Wanner, *Geometric Numerical Integration: Structure-Preserving Algorithms for Ordinary Differential Equations*, Springer Science, London, 2006. Available from: https://link.springer.com/book/10.1007/3-540-30666-8.

26. H. Li, Y. Wang, M. Qin, A sixth order averaged vector field method, *J. Comput. Math.*, **34** (2016), 479–498. https://doi.org/10.4208/jcm.1601-m2015-0265

27. Q. Hong, Y. Wang, J. Wang, Optimal error estimate of a linear Fourier pseudo-spectral scheme for two-dimensional Klein-Gordon-Schrödinger equations, *J. Math. Anal. Appl.*, **468** (2018), 817–838. https://doi.org/10.1016/j.jmaa.2018.08.045

28. J. Wang, A. Xiao, Conservative Fourier spectral method and numerical investigation of space fractional Klein-Gordon-Schrödinger equations, *Appl. Math. Comput.*, **350** (2019), 348–365. https://doi.org/10.1016/j.amc.2018.12.046

29. J. Macías-Díaz, A structure-preserving method for a class of nonlinear dissipative wave equations with Riesz space-fractional derivatives, *J. Comput. Phys.*, **351** (2017), 40–58. https://doi.org/10.1016/j.jcp.2017.09.028

30. J. Macías-Díaz, A numerically efficient dissipation-preserving implicit method for a nonlinear multidimensional fractional wave equation, *J. Sci. Comput.*, **77** (2018), 1–26. https://doi.org/10.1007/s10915-018-0692-z

31. J. Macías-Díaz, A. Hendy, R. Staelen, A compact fourth-order in space energy-preserving method for Riesz space-fractional nonlinear wave equations, *Appl. Math. Comput.*, **325** (2018), 1–14. https://doi.org/10.1016/j.amc.2017.12.002

32. D. Hu, W. Cai, Y. Song, Y. Wang, A fourth-order dissipation-preserving algorithm with fast implementation for space fractional nonlinear damped wave equations, *Commun. Nonlinear Sci. Numer. Simul.*, **91** (2020), 105432. https://doi.org/10.1016/j.cnsns.2020.105432

33. D. Hu, Y. Gong, Y. Wang, On convergence of a structure preserving difference scheme for two–dimensional space–fractional nonlinear Schrödinger equation and its fast implementation, *Comput. Math. Appl.*, **98** (2021), 10–23. https://doi.org/10.1016/j.camwa.2021.06.018

34. Z. Sun, Y. Liu, B. Yin, H. Li, Fast structure-preserving difference algorithm for 2D nonlinear space-fractional wave models, *Comput. Math. Appl.*, **123** (2022), 40–58. https://doi.org/10.1016/j.camwa.2022.07.020

35. N. Wang, M. Li, C. Huang, Unconditional energy dissipation and error estimates of the SAV Fourier spectral method for nonlinear fractional generalized wave equation, *J. Sci. Comput.*, **88** (2021), 19. https://doi.org/10.1007/s10915-021-01534-8

36. J. Yan, Z. Zhang, New energy-preserving schemes using Hamiltonian boundary value and Fourier pseudospectral methods for the numerical solution of "good" Boussinesq equation, *Comput. Phys. Commun.*, **201** (2016), 33–42. https://doi.org/10.1016/j.cpc.2015.12.013

37. Y. Gong, J. Zhao, X. Yang, Q. Wang, Fully discrete second-order linear schemes for hydrodynamic phase field models of binary viscous fluid flows with variable densities, *SIAM J. Sci. Comput.*, **40** (2018), B138–B167. https://doi.org/10.1137/17M1111759

38. X. Yang, Linear, first and second-order, unconditionally energy stable numerical schemes for the phase field model of homopolymer blends, *J. Comput. Phys.*, **327** (2016), 294–316. https://doi.org/10.1016/j.jcp.2016.09.029

39. J. Shen, J. Xu, J. Yang, The scalar auxiliary variable (SAV) approach for gradient flows, *J. Comput. Phys.*, **353** (2018), 407–416. https://doi.org/10.1016/j.jcp.2017.10.021

40. J. Shen, J. Xu, Convergence and error analysis for the scalar auxiliary variable (SAV) schemes to gradient flows, *SIAM J. Numer. Anal.*, **56** (2018), 2895–2912. https://doi.org/10.1137/17M1159968

41. Y. Fu, D. Hu, Y. Wang, High-order structure-preserving algorithms for the multi-dimensional fractional nonlinear Schrödinger equation based on the SAV approach, *Math. Comput. Simul.*, **185** (2021), 238–255. https://doi.org/10.1016/j.matcom.2020.12.025

42. Y. Fu, Z. Xu, W. Cai, Y. Wang, An efficient energy-preserving method for the two-dimensional fractional Schrödinger equation, *Appl. Numer. Math.*, **165** (2021), 232–247. https://doi.org/10.1016/j.apnum.2021.02.010

43. C. Jiang, Y. Wang, Y. Gong, Arbitrarily high-order energy-preserving schemes for the Camassa-Holm equation, *Appl. Numer. Math.*, **151** (2020), 85–97. https://doi.org/10.1016/j.apnum.2019.12.016

44. Z. Liu, X. Li, The exponential scalar auxiliary variable (E-SAV) approach for phase field models and its explicit computing, *SIAM J. Sci. Comput.*, **42** (2019), B630–B655. https://doi.org/10.1137/19M1305914

45. Y. Wang, B. Wang, M. Qin, Local structure-preserving algorithms for partial differential equations, *Sci. China Ser. A-Math.*, **51** (2008), 2115–2136. https://doi.org/10.1007/s11425-008-0046-7

46. C. Jiang, W. Cai, Y. Wang, A linearly implicit and local energy-preserving scheme for the sine-Gordon equation based on the invariant energy quadratization approach, *J. Sci. Comput.*, **80** (2019), 1629–1655. https://doi.org/10.1007/s10915-019-01001-5

47. Y. Gong, J. Cai, Y. Wang, Some new structure-preserving algorithms for general multi-symplectic formulations of Hamiltonian PDEs, *J. Comput. Phys.*, **279** (2014), 80–102. https://doi.org/10.1016/j.jcp.2014.09.001

48. Y. Li, X. Wu, General local energy-preserving integrators for solving multi-symplectic Hamiltonian PDEs, *J. Comput. Phys.*, **301** (2015), 141–166. https://doi.org/10.1016/j.jcp.2015.08.023

49. Y. Zhou, *Application of Discrete Functional Analysis to the Finite Difference Methods,* International Academic Publishers, Beijing, 1990.

50. E. Celledoni, V. Grimm, R. I. McLachlan, D. I. McLaren, D. O'Neale, B. Owren, et al., Preserving energy resp. dissipation in numerical PDEs using the "Average Vector Field" method, *J. Comput. Phys.*, **231** (2012), 6770–6789. https://doi.org/10.1016/j.jcp.2012.06.022

51. S. Reich, Multi-symplectic Runge-Kutta collocation methods for Hamiltonian wave equations, *J. Comput. Phys.*, **157** (2000), 473–499. https://doi.org/10.1006/jcph.1999.6372

52. C. Schober, T. Wlodarczyk, Dispersive properties of multisymplectic integrators, *J. Comput. Phys.*, **227** (2008), 5090–5104. https://doi.org/10.1016/j.jcp.2008.01.026

53. W. Cai, C. Jiang, Y. Wang, Y. Song, Structure-preserving algorithms for the two-dimensional sine-Gordon equation with Neumann boundary conditions, *J. Comput. Phys.*, **395** (2019),166–185. https://doi.org/10.1016/j.jcp.2019.05.048

AIMS Press